

The application of electroanalytical methods to the analysis of phase transitions during intercalation of ions into electrodes

M. D. Levi · D. Aurbach

Received: 5 September 2006 / Revised: 23 October 2006 / Accepted: 8 December 2006 / Published online: 1 March 2007
© Springer-Verlag 2007

Abstract Mechanisms of first-order phase transition induced by electrochemical intercalation of Li ions into composite graphite electrode are studied both theoretically, in the framework of lattice gas models, and experimentally, by a combination of electroanalytical techniques, such as cyclic voltammetry, potentiostatic intermittent titration (PITT), galvanostatic intermittent titration (GITT), and electrochemical impedance spectroscopy (EIS). From the analysis of the mismatch between the accessible phase-transition rate constants and the characteristic time windows for various electroanalytical methods, we conclude that only a combined application of these techniques provides sufficient, self-consistent information on the mechanisms of phase transitions in graphite electrodes. The advantages and disadvantages in using these techniques are discussed. PITT with a small potential step is the most appropriate tool for measuring the entire sequence of rate-determining steps of phase transitions as a function of time. The latter technique can be conveniently used for quantitative analysis of slow nucleation and the growth of new phases in the bulk of the old one, followed by the coalescence of nuclei and the formation of phase boundaries between the coexisting phases. The movement of this boundary into the electrode's bulk has been properly modeled in terms of two alternative models.

Keywords PITT · GITT · EIS · Li-ion batteries · Intercalation · Nucleation and growth · Diffusion · Differential intercalation capacitance · Chemical diffusion coefficient

Introduction

The charging and discharging of rechargeable Li-ion batteries involves Li-ion transfer from one ion insertion electrode (IIE) to another one [1, 2]. This transfer can be considered as a topotactic intercalation reaction, meaning that the guest ions occupy the interstitial sites of both crystalline host matrices and that their charging and discharging result in a nonuniform concentration profile in the electrodes' bulk, thus, separating the coexisting phases with different concentrations of guest ions [3]. The coexistence of different phases during ion insertion has been repeatedly confirmed by in situ X-ray diffraction (XRD) characterizations for a large variety of IIEs [4–7]. The process of ion insertion into host electrodes that have been polarized in solutions can be regarded as first-order phase transition [8]. An alternative to first-order phase transition is the solid-solution type of intercalation reaction, which implies a uniform (monotonous) concentration profile of guest ions in the electrode bulk, and as a consequence, the output of the intercalation reaction is a single phase with a potential-dependent concentration of ions. One of the most critical differences between the electrochemical behaviors of these two extreme types of insertion electrodes is the fact that the former type of electrode does not reach a true equilibrium state during the entire process of ion insertion.

The thermodynamic driving force for phase transition during ion intercalation has been previously discussed within the framework of lattice gas models by McKinnon

“Contribution to the International Workshop on Electrochemistry of Electroactive Materials (WEEM-2006), Repino, Russia, 24–29 June 2006.”

M. D. Levi (✉) · D. Aurbach
Department of Chemistry, Bar-Ilan University,
Ramat Gan 52900, Israel
e-mail: levimi@mail.biu.ac.il

and Haering [8], by Feldberg and Rubinstein [9], and by Vorotyntsev and Badiali [10]. These research groups clearly demonstrated that highly attractive short-range interactions between the intercalation sites result in the appearance of a high maximum on the nonequilibrium electrochemical free energy curve as a function of the intercalation level. However, as thermodynamic analysis does not provide an answer to the question of what kind of relaxation processes determine the rate of phase transition, kinetic analysis is required. McKinnon and Haering [8] have suggested that slow solid-state diffusion is, presumably, the rate-determining step (RDS) for phase transition. In contrast, Vorotyntsev and Badiali [10] have concluded that both the slow interfacial charge transfer (Butler–Volmer kinetics) and the nonuniform character of the intercalation process result in the formation of small, energetically more favorable droplets of new phase in the bulk of the old one.

The appearance of two minima on the free energy curve vs intercalation level separated by a high energetic barrier means that two phases, with substantially different ion concentrations, can exist concurrently, provided that the free energy barrier is overcome by a suitable relaxation process. Indeed, two-phase coexistence during ion insertion into host electrodes has been confirmed not only by appropriately designed *in situ* XRD characterizations [4, 5] but also, in suitable cases, by direct observation of the moving boundary, which indicated the different colors of the lithiated graphite in various stages (see Funabiki et al. [11]). Both Funabiki and Shin Heon-Cheol et al. [12, 13] have elaborated on their findings with models that quantitatively describe such a movement.

Using a phase-field model, Han et al. [3] have recently presented a comprehensive view of how the existence of the spinodal domain in the free energy curve affects the applicability of classical electroanalytical techniques for the determination of the chemical diffusion coefficient, D . In other words, they took into account the effect of the distinct boundary between the coexisting phases (infinitely high concentration gradient) on the free energy curve and the expression of the ions' flux. This leads to a correction of the classical Fick's law, which postulates dependence on the energy gradient coefficient that characterizes the phase separation. Numerical estimates of the dependence of D on the insertion level (from the generalized Fick's law), using reasonably adapted values of the energy gradient coefficient, have led to a general conclusion that incremental titration techniques such as potentiostatic intermittent titration (PITT) and, in particular, galvanostatic intermittent titration (GITT)—which have been known to be limited to the case of a uniform concentration profile in the electrode (i.e., assuming the validity of the classical Fick's law)—are still valid for the metastable domain, in close proximity to the spinodal domain itself.

Starting from a model-based evaluation of the effect of slow nucleation on the shape of cyclic voltammetric response, we then extended it further to modeling the chronoamperometric response of intercalation electrodes [14–20]. This yielded a much better separation between the contributing RDS of phase transition. A question arises as to how electrochemical methods reflect the different kinetic limiting stages of phase transitions during the intercalation of ions into electrodes. This is an important issue, especially for material science researchers who use classic electrochemical techniques that are directly implemented for kinetic analysis of phase transitions. The major difficulty lies in selecting the appropriate technique and in the consistency between the results obtained by simultaneous (or parallel) application of different relaxation techniques. For example, whereas a chronoamperometric study could, in appropriate cases, provide direct evidence for nucleation and the growth of a new phase in the bulk of the old one, it is not, *a priori*, clear as to how the related phenomenon might be reflected by parallel cyclic voltammetry (CV) or which frequency domain of an impedance spectrum should be the focus of research. Special attention should be paid to the capability of electrochemical impedance spectroscopy (EIS) to reflect the kinetic features of phase transition in the low-frequency domain, and in addition, attention should be given to the correlation of this behavior with the behavior of the chronoamperometric curves in their long-time domains or slow scan rate CV. Based on our previous publications [14–20], this short review provides some initial insight into these problems.

The paper is organized as follows. In “Non-equilibrium free energy curves during phase transition caused by ion insertion” of the Results and Discussion chapter, we review the mean-field approximation of the nonequilibrium electrochemical free energy of the intercalation process with highly attractive, short-range interactions between the intercalated ions. The connection between the free energy curve and the chemical potential for the inserted ions, the type of intercalation isotherm, and the equilibrium characteristics of the electrodes are discussed in detail. Selected CV and chronoamperometric studies of Li insertion into graphite electrodes (“Non-equilibrium free energy curves during phase transition caused by ion insertion” and “General features of the chronoamperometric response of graphite electrodes during LiC_{12} to LiC_6 phase transition and application of the electrocrystallization model”, respectively) demonstrate unequivocally that the above-mentioned equilibrium scenario of phase transition is *not realized in practice*, and the different relaxation processes control the rate of phase transition as time elapses. We then further show that a new phase appears within the bulk of the old one through the formation of small droplets. These, in turn, coalesce and finally form a distinct phase boundary that moves in time towards the electrode's mass. “Pseudo-

Cottrellian vs moving boundary model for a description of phase transition” deals with the quantitative description of this movement and its interpretation in terms of the moving boundary and the alternative Cottrellian model. Finally, in “The mismatch between the accessible rate constants of different kinetic stages of phase transition and the characteristic time windows of the electrochemical techniques,” we show how the account of small droplets formation reduces the energetic barrier and modifies accordingly the shape of the charging (discharging) curves. The respective applications of CV, PITT, GITT, and EIS to the study of phase transitions are compared in this section, taking into account the different accessible rate constants of the kinetic steps of the phase transition and the different time windows inherent in the above electrochemical techniques.

Experimental

First-order phase transitions in IIEs result in very steep charging and discharging curves (charge vs potential), and thus, the best resolution of data with respect to potential is required. This can be reached with a thin, low mass film or powdery composite electrodes in contact with a small amount of suitable electrolyte solutions. A good practical choice is a coin-type cell configuration in which parasitic background currents are relatively low because of the high ratio between the electrodes’ surface area and the small volume of the electrolyte solution (see a comparison of the electroanalytical features of the lithiated graphite in coin-type cells and in large, flooded cells [21]). The preparation of thin composite graphite electrodes has been described previously [14, 15, 21]. The electrodes used here for room temperature measurements contained ~1.8 mg of graphite powder (KS-15 from Timrex) and 10% (by weight) PVdF binder. The cells were standard 2032 coin-type cells (NRC, Canada), containing the composite graphite working electrode (of a geometric area of 1.5 cm²), Li counter- and reference electrodes (CE and RE, respectively). The separator was a Cellgard polypropylene membrane placed between the Li CE and RE, whereas a thin sheet of glassy paper separated the working electrodes (WE) and the RE. A thin strip of Li RE was pressed onto a Ni wire and carefully isolated from both WE and CE and from the stainless steel framework by a thin polypropylene tape (for details see [21]) The cells were constructed under a highly pure argon atmosphere in VAC glove boxes and were hermetically sealed by a standard crimping device (NRC) and additionally isolated with epoxy resin. The cells were thermostated with an accuracy of ±0.1 °C.

The electrolyte solution was 1 M LiPF₆ in an ethylene carbonate + dimethylcarbonate 1:1 mixture (Li-battery grade from Merck, KGaA).

PITT and GITT were applied using a computerized potentiostat–galvanostat Model 20 Autolab, from Eco Chemie, which included a FRA module. The collection of data was controlled by the GPES Version 4.9 Eco Chemie B.V. Software (Utrecht, The Netherlands).

For potentiostatic titration of graphite electrodes, potential steps of variable amplitude were used, namely, several tens of millivolts and only several millivolts in the potential regions between and inside the differential capacitance peaks, respectively. The duration of each potential step was long enough to enable the reaching of full equilibration of the electrodes so that the current at the end of a step was less than 0.5% of its initial value (typical equilibration time was several tens of minutes and several hours in the potential regions between and inside the differential capacitance peaks, respectively). Up to 35 titrations were performed both for Li-ion insertion (intercalation) and deinsertion (deintercalation).

GITT procedure was used by applying a current pulse of 27.7 μA for 2,400 s. The amount of the injected charge was usually 3.3% of the total electrode capacity, and thus, approximately 30 titrations were performed for both Li-ion insertion and deinsertion. The time of relaxation after each current pulse was 2 h.

EIS was performed at predefined potentials, using an AC voltage amplitude of 5 mV after the prepolarization at the same potentials for a period of 20–30 min.

Results and discussion

Non-equilibrium free energy curves during phase transition caused by ion insertion

As the insertion process can be viewed, to a first approximation, as an adsorption of guest particles onto the host lattice, it can be conveniently described in the framework of the lattice gas model with short-range interactions between the intercalation species. We start the analysis by considering, initially, the nonequilibrium electrochemical free energy of an intercalation process. Figure 1 shows, as an example, the plots of dimensionless nonequilibrium electrochemical free energy per unit site, F_i/kTc_m vs intercalation level, x , calculated for the different potentials ($E-E_0$) [10, 15]:

$$\frac{\Delta F}{kTc_{Li^+}} = -fx\Delta(E - E_0) + x \ln x + (1 - x) \ln(1 - x) - 0.5gx(1 - x). \quad (1)$$

In this study, c_{Li^+} is the maximal concentration of Li ions in the electrode bulk; x is the dimensionless level of

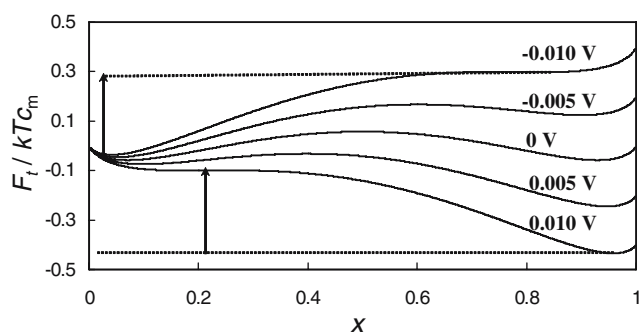


Fig. 1 Nonequilibrium free energy per unit site, F_i/kTc_m , vs intercalation level, x , Eq. 1, for $g=-6$ and the values of potential, $(E-E_0)$, indicated on each curve

Li-ion intercalation; k and T are the Boltzmann constant and the absolute temperature, respectively; f is the combination of k , T , and the electronic charge; and e : $f = e/kT$. E and E_0 are the electrode potential and its standard value, respectively. For simplicity, we consider the case of short-range ion–ion interactions only, disregarding the electron–electron and electron–ion interactions, which is approximately valid for IIEs with high electronic conductivity [15].

The shape of the free energy curve vs the intercalation level depends strongly on the effective dimensionless interaction parameter g . In the case of the absence of ion–ion interactions, $g=0$. Under this circumstance, the Frumkin insertion isotherm reduces to a Langmuirian-type isotherm [10, 15–17]). The cases $g>0$ and $g<0$ are characteristic of the repulsive and the attractive interactions, respectively. When $g=-4$, the highly attractive interactions between the intercalation sites force the reaction to proceed as an ideal first-order phase transition at the standard potential.

All of the mean-field free energy curves are shown in Fig. 1 as functions of potential for the particular case of a highly attractive interaction with $g=-6$. We will first consider the deintercalation reaction (charging) when the electrode potential is swept towards more positive values. It is immediately seen from the curves in Fig. 1 that, at $E-E_0<0$, a rather high maximum (hump) appears, which separates two minima with low and high ionic concentrations, respectively. This barrier remains even at $E-E_0=0$ and starts to degrade with the further anodic polarization in a very narrow potential range: at $E-E_0=10$ mV, the hump completely disappears, thus initiating a deintercalation reaction. The intercalation reaction (as $E-E_0$ shifts in the negative direction) can be regarded as the inverse process to the deintercalation reaction, as is easily seen from Fig. 1: at $E-E_0=10$ mV, the curve has a high hump, which also remains at $E-E_0=0$; complete elimination of this peak occurs at $E-E_0=-10$ mV.

Differentiation of Eq. 1 with respect to intercalation level, x , results in a simple Frumkin-type isotherm of the form [15]:

$$f(E-E_0) = \ln\left(\frac{x}{1-x}\right) + g(x-0.5). \quad (2)$$

When calculated with $g=-6$, the charging and discharging curve shows a clear N-shaped feature around the standard potential (see Fig. 2). Such a shape of charging and discharging curves is rather hypothetical: To be realized on a practical basis, one should assume that intercalated ions may overcome the hump on the free energy curve relatively quickly. However, the kinetics of all known up-to-date relaxation processes (characteristic of intercalation reactions) are hardly rapid enough to overcome such high energetic barriers.

It is of interest to analyze the shape of the ideal differential intercalation capacity curve, C_{dif} , and the chemical diffusion coefficient, D , as functions of x for highly attractive interactions between the intercalation sites. The former quantity can be easily obtained by differentiation of Eq. 2 with respect to x [15]:

$$\frac{C_{\text{dif}}}{fQ_m} = \left(g + \frac{1}{x} + \frac{1}{1-x}\right)^{-1}, \quad (3)$$

whereas the latter one takes the following simple form [8, 15]:

$$\frac{D}{D_0} = [1 + gx(1-x)]. \quad (4)$$

Here, Q_m and D_0 are the maximum available intercalation charge and the intrinsic (or component) diffusion coefficient, respectively.

Figure 3a and b shows the plots of C_{dif}/fQ_m and D/D_0 vs x , respectively, for $g=-4.2$. From panel a, it is seen that the charging process begins when x approaches 0.4. When x is exactly equal to 0.4, the differential capacity runs to $+\infty$ and $-\infty$ on its left and right limits, respectively. As x further increases to 0.5, the differential capacity decreases

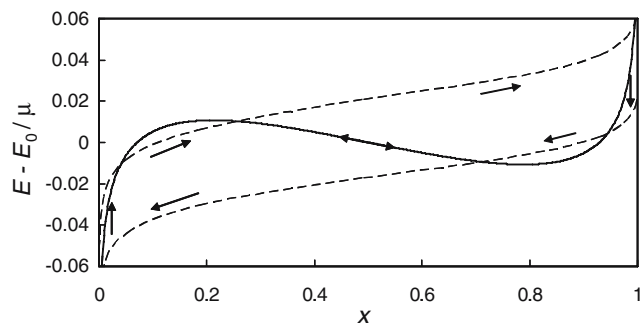


Fig. 2 Quasi-equilibrium, ideal type of charge and discharge of an intercalation electrode exhibiting a phase transition with $g=-6$ (solid N-shaped line). Broken lines show theoretical charge and discharge curves due to a slow nucleation mechanism (Eq. 14): $n=4$, $\nu=10$ $\mu\text{V s}^{-1}$, $\omega=10^{-2}$ s^{-1}

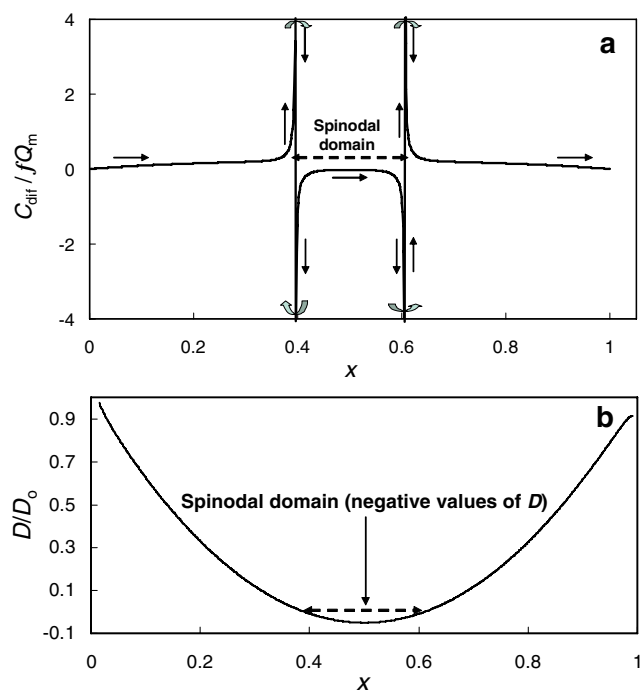


Fig. 3 Plots of the quasi-equilibrium differential capacity of an intercalation electrode vs intercalation level x (a) and the ideal dependence of D vs x (b) calculated from equations 3 and 4, respectively, for $g=-4.2$. The spinodal domain is shown in both graphs

in absolute value while still retaining its negative sign. As x increases from 0.5 to 1, the differential capacity curve manifests full symmetry with respect to $x=0.5$. The range of x between 0.4 and 0.6, in which C_{dif} is negative, is called the spinodal domain [3] and corresponds to the middle part of the N-shaped charging–discharging curve in Fig. 2. As seen from the parallel graph in panel b, the spinodal domain is also characterized by negative values of the chemical diffusion coefficient.

It should be mentioned that the above scenario of quasi-reversible charging and discharging of a host material cannot be practically realized in view of high barriers in the free energy curves that separate the phases with low and high concentrations of ions. There should be other, presumably, nonuniform distributions of ions in the host matrix [10], which facilitate the transfer across the free energy hump described above.

To take a glance at the nature of the RDS involved in phase transitions, we refer to CV curves measured from a composite graphite electrode at potential scan rates decreasing from 50 to 10 $\mu\text{V s}^{-1}$ (see Fig. 4). It is seen that both cathodic and anodic peaks approach the middle-peaks (i.e., standard) potential of the related couples. The most prominent of these are the peaks due to $\text{LiC}_{12}/\text{LiC}_6$ (phase 2/phase 1) couples, marked as A and A' , respectively, (peaks of lower heights, B/B' and C/C' , are due to phase 3/phase 2 and diluted phase 1/phase 4 transitions, respectively). Simultaneously, the peaks

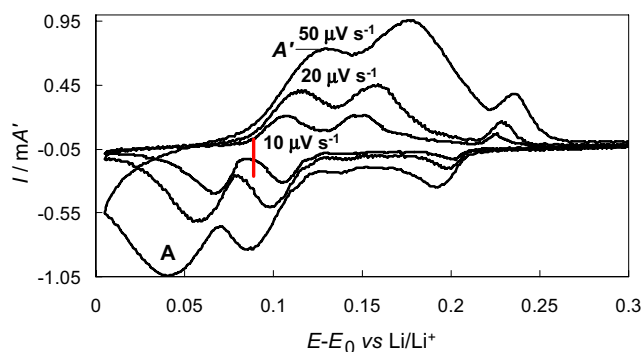


Fig. 4 Typical cyclic voltammetry curves measured from a composite graphite electrode (1.7 mg active mass) at different scan rates. The red line marks the range of potentials from 0.085 to 0.080 V, in which almost complete conversion of phase 2 to phase 1 takes place during intermittent titration. CV peaks denoted as A/A' , B/B' , and C/C' relate to phase II/phase I, phase III/phase II, and diluted phase 1/phase IV transitions, respectively

become narrower, as the scan rate decreases. Earlier, we presented clear evidence that, in the range of the relatively high scan rates, limitations due to slow solid-state diffusion (i.e., diffusion of ions in the host matrix) together with high ohmic drops may limit the rate of phase transition during lithiation of graphite [20]. Of course, the scan rate may be decreased to several microvolts per second, thus, eliminating diffusion as an apparent RDS [15]. However, in any case, CV is a large-amplitude technique and, therefore, does not allow us to monitor the different relaxation processes in the very narrow potential range in which phase transition takes place (as outlined above). This should be interpreted as a mismatch between the required rate constant of the intercalation kinetics and the characteristic time window of the CV experiment. Small-amplitude incremental titrations of IIEs should solve the above mismatch and, thus, be far more appropriate for this purpose. To visualize the problem under consideration, in Fig. 4, we used a red line to mark a small potential step from 0.085 to 0.080 V (vs Li/Li^+) in which the entire phase 2-to-phase 1 transition takes place. It is seen that this potential region is several tens of millivolts more positive, compared to the location of peak A , measured even at the slowest scan rate of 10 $\mu\text{V s}^{-1}$. This shows that the different electrochemical methods reflect different relaxation processes associated with the phase transition. It is worthwhile to discuss in greater detail a unique resolution of the chronoamperometry as concerns the temporal sequence of different RDS during phase transition.

General features of the chronoamperometric response of graphite electrodes during LiC_{12} to LiC_6 phase transition and application of the electrocrystallization model

Figure 5 shows the chronoamperometric response to potentiostatic titration of a composite graphite electrode between 0.085 and 0.080 V. Typically, five different

domains are clearly seen in this figure. In the first, a short-time domain denoted as I, the current drastically decreases to a minimum and then increases (domain II). A broad maximum of current is observed (the boundary between the domains II and III), and then, the current gradually begins to decrease (domain III). This decrease continues within domain IV, marked by an increase in $-dI/dt$, and finally, the current drops to a very small value over longer periods of time when the electrode reaches complete equilibrium with Li ions in the solution at the applied potential of 0.080 V (domain V marked by a decrease in $-dI/dt$). Domains I, II, and III are well separated (by a minimum and maximum in current, respectively, in Fig. 5), whereas the boundaries between domains III, IV, and V were obtained from the application of a moving boundary model, as explained below.

Full assignments of all of the five domains were already presented elsewhere [19]. In brief, we assume that two major events (in addition to the double-layer charging) occur in domain I: (1) The initial phase, stage 2 (i.e., LiC_{12}), is saturated with the inserted Li ions, so that nuclei with a *subcritical* size may form after this saturation; (2) These subcritical size nuclei have a limited probability of being formed. They then coalesce to form larger size, *supercritical* nuclei. The current in domain I reflects this scenario and thereby decreases relatively slowly as the subcritical LiC_6 nuclei reach the maximal concentration that stage II can contain. The formation of supercritical nuclei is a well-documented fact in the field of metal electrocrystallization [22, 23]. However, most important for our consideration is domain II, with an approximately linear increase in current with time. Once again, by analogy with the electrocrystallization of metals on foreign substrates [24, 25], we assumed that the growth of the supercritical nuclei, accompanied by an increase in their surface area, is

the reason for the increase in current measured in domain II (Fig. 5) [26]. These supercritical nuclei are formed in the electrode near its boundary with the electrolyte solution and gradually increase in size, overlapping with each other and finally forming a continuous phase (stage 1). This phase is located between the contact of the electrode with the electrolyte solution and the boundary between the two coexisting stages 1 and 2 in the electrode bulk.

For growing cylindrical nuclei (far from where they overlap within the graphite particles), the common electrocrystallization models [24, 25] predict a linear dependence of I on t of the type:

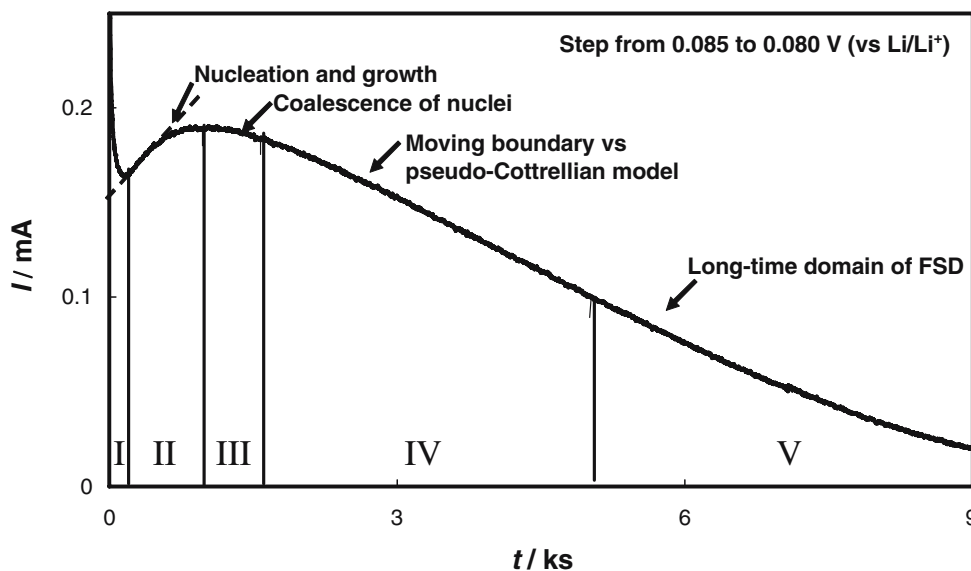
$$I = \frac{2nFbA}{M} (\pi N_o a^2) t, \quad (5)$$

where n , F , A , and M denote the number of electrons participating in the insertion reaction, the Faraday number, the active surface area of the electrode, and the atomic mass of the inserted Li, respectively. N_o is the total number of nucleation sites in the “nucleation layer” of the electrode, and a is the lateral growth velocity (in centimeter per second). The quantity b defines a mass per surface unit characteristic of the first insertion layer of Li ions:

$$b = \frac{\Delta Q M}{nFA}. \quad (6)$$

Thus, the physical reason for the increase in current with time is the increase in the total surface area of nuclei of the new phase through which the current passes. This was also confirmed by GITT and by the relaxation of OCV after the application of large current pulses [18]. For the sake of brevity, and as we are going to concentrate attention on the subsequent steps of phase transition (domains III and IV), we omit discussion of the physical reliability of the

Fig. 5 Plot of the current, I , vs time, t , obtained by intermittent titration of graphite electrode across the major intercalation peak ($\text{LiC}_{12} \rightarrow \text{LiC}_6$), potential step from 0.085 to 0.080 V. Five characteristic domains are indicated



estimated parameters (including their temperature dependence), see [26]. The coalescence of nuclei of the new phase marks the end of the growth of the total surface area. For this reason, the current increases to a maximum in domain III. The current further decreases within domain IV, which we assign to the advancement of the boundary between the two coexisting phases towards the electrode’s bulk.

Pseudo-Cottrellian vs moving boundary model for a description of phase transition

In a paper published elsewhere [26], we tried to describe quantitatively the decline of the current in domain IV by two alternative models: (1) a progressive movement of the boundary (adapted from the earlier work of Funabiki et al. [11]) and (2) the model based on a quasi-Cottrellian approach. The difference between the two models can be immediately recognized from the advancement of the concentration profiles with time as intercalation proceeds.

We consider a square platelet graphite particle in which ion insertion takes place from two opposite sides only (from left and right towards the particle’s interior; see upper parts of panels a and b in Fig. 6). The initial concentration of Li ions in phase 2 is c_0 (see lower parts of panels a and b in Fig. 6). We first consider the quasi-Cottrellian model (panel a). The nucleation step cannot be accounted for in this approach, so we adopt the assumption that the initial time for the appearance of a concentration gradient coincides with the characteristic time of the maximum in domain II, t_m (i.e., the corrected time t' is introduced: $t' = t - t_m$). Within the Cottrellian approach, the experimentally determined ratio Q_t/Q_∞ (i.e., the ratio of the injected charge at each moment of time t' (Q_t) to the total charge (Q_∞) at the infinite time $t' = \infty$) is proportional to the square root of time (see Eq. 50 in [27]):

$$\frac{Q_t}{Q_\infty} = 2 \left(\frac{t'}{\pi \tau_d} \right)^{1/2} \tag{7}$$

where the diffusion time constant $\tau_d = l^2/4D$, as we consider the diffusion from two opposite edges of the particle. The diffusion layer thickness, δ , is equal to [28]:

$$\delta = (\pi D t')^{1/2} \tag{8}$$

Thereby, a combination of Eqs. 7 and 8 provides a connection between δ and the experimental ratio Q_t/Q_∞ within the Cottrellian model:

$$\delta = \frac{Q_t}{Q_\infty} \frac{l\pi}{4}. \tag{9}$$

Equation 9 shows that the Cottrellian model predicts a linear dependence of δ on Q_t/Q_∞ . This ratio gradually

decreases with time; however, as time elapses, the semi-infinite diffusion domain is changed by a finite-space domain, so that the bulk concentration of guest ions increases accordingly (see lower panel b in Fig. 6).

Surprisingly, the alternative moving boundary model also predicts a linear dependence of its location within the platelet particle with time, $\xi(t)$ (see the upper panel b in Fig. 6). The ratio of the injected charge at each moment of time t' (Q_t) to the total charge (Q_∞) at the infinite time $t' = \infty$ can be expressed through the ratio of the surface of two rectangular figures related to the new phase 1 and to the total surface of the square (Fig. 6b). Hence, the location of the moving boundary can be determined from the following simple equation:

$$\frac{Q_t}{Q_\infty} = \frac{l - (l - 2\xi)}{l}, \quad (0 < \xi < l/2) \tag{10}$$

and, hence, ξ is proportional to $\frac{Q_t}{Q_\infty}$:

$$\xi = \frac{Q_t l}{Q_\infty 2}. \tag{11}$$

The position of the moving boundary at $t' > 0$ (which separates the coexisting phases) is schematically shown in Fig. 6b. To link ξ to the diffusion coefficient D , we use herein, following Funabiki et al. [11], the Wagner approach to diffusion in a binary system containing a phase boundary. Wagner assumed that phase boundaries move linearly with $t'^{1/2}$:

$$\xi = 2\gamma(D_1 t')^{1/2} \tag{12}$$

where γ is the dimensionless parameter (which was estimated as 0.52; for details see [19]), and D_1 is the diffusion coefficient for the propagating phase (i.e., of phase 1, in the case under consideration). Note that the component, rather than the chemical diffusion coefficient, is here implied [11].

From a comparison of Eqs. 9 and 11, one can easily see that the location of δ and ξ differ by a time-independent constant only. Substituting $\gamma = 0.52$ in Eq. 2 and taking into account the experimental slope of the ξ vs $t'^{1/2}$ plot ($k' = 0.057 \mu\text{m s}^{-1/2}$), one readily obtains from the moving boundary model that $D_1 = 3.0 \times 10^{-11} \text{ cm}^2 \text{ s}^{-1}$. On the other hand, from a combination of Eqs. 8 and 9, we obtain in the framework of the pseudo-Cottrellian model the diffusion coefficient $D = 2.5 \times 10^{-11} \text{ cm}^2 \text{ s}^{-1}$, which is very close to the above value, $D = 3.0 \times 10^{-11} \text{ cm}^2 \text{ s}^{-1}$, which followed from the moving boundary model.

Despite the similarity between the values of D obtained by two alternative models, it is worthwhile to examine these values in the context of the dependence of D on the whole intercalation region, from diluted to concentrated phase 1. Using a quasi-Cottrellian approach, we calculated

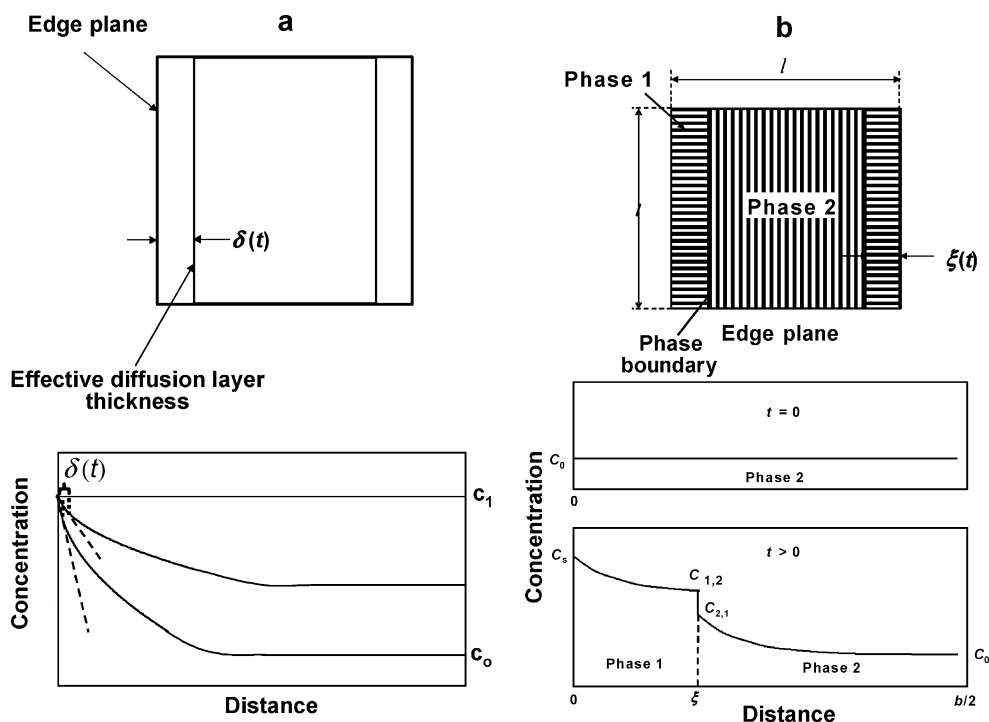


Fig. 6 A simple geometric model used for determining the time dependence of the moving boundary location, ξ , formed during electrochemical conversion of the staged graphite phase 2 to 1 (top of panel b). **a** Reproduction of an alternative pseudo-Cottrellian approach to treatment of chronoamperometric data. The location of the time-dependent effective diffusion layer thickness, δ , is indicated. **b** Schematic view of the concentration profiles along the moving boundary in a graphite particle (bottom panel): (1) pure phase 2 (prior to the application of the potential step, $t=0$) and (2) during the potential step towards the formation of phase 1 ($t>0$). The straight line

marks the position of the moving boundary (ξ); the concentrations at the surface (in contact with an electrolyte solution), c_s , in graphite particle bulk, c_o , and on both sides of the moving boundary ($c_{1,2}$ and $c_{2,1}$) are indicated. Schematic representation of the concentration profile after application of a potential step according to a pseudo-Cottrellian model is shown at the bottom of panel a. As the intercalation reaction proceeds, the thickness of the diffusion layer δ increases with time, whereas the bulk concentration of ions rises from c_o (phase 2) to c_1 (phase 1)

$D=l^2/\tau_d$ during potentiostatic titration, according to the equation [15, 29, 30]:

$$\tau_d(E) = \left[\frac{C_{\text{dif}}}{\pi^{1/2} \left(\frac{l^2}{\Delta E} \right)} \right] \quad (13)$$

In this approximation, contributions other than slow solid-stated diffusion are ignored. The results related to a composite graphite electrode are presented by a curve in Fig. 7 (marked by open circles). The above assumption is, in a sense, unrealistic, and ohmic drops, as well as slow interfacial kinetics, may well contribute to the total chronoamperometric response and, consequently, be responsible for the so-called spurious behavior of D in the vicinity of E_0 , i.e., close to the peak of C_{dif} (see recent discussions in [31–33]). For this reason, we used a two-step method to correct the values of D , taking into consideration the involvement in the current response of the above ohmic and slow kinetics contributions [34, 35]. The corrected values of D are shown in Fig. 7 by the upper curve marked by solid circles. For pure phases, the corrected values of D

appeared to be approximately one order of magnitude higher than the uncorrected ones.

The validity of the quasi-Cottrellian approach was independently proved by the following comparison. Funabiki et al. [36] determined the values of D for insertion of Li ions into highly oriented pyrolytic graphite (HOPG). The characteristic diffusion length for Li ions in the HOPG electrode was precisely determined [36]. From Fig. 7, it is seen that D for the dilute phase 1 and phase 4 obtained with HOPG electrode (marked by the broken horizontal lines)

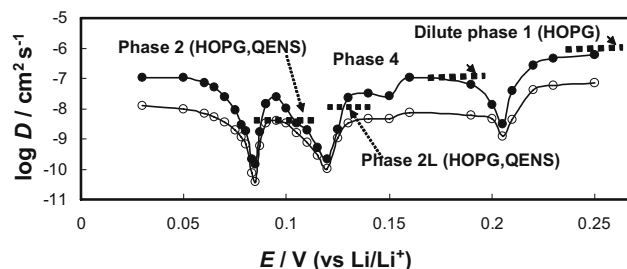


Fig. 7 Plots of the chemical diffusion coefficient, $\log D$, as a function of the electrode potential, E , obtained for a composite graphite electrode by PITT both for Li ions insertion (for details, see the text)

are in very good agreement with the refined values of D for our composite, powdery graphite electrode. This shows that the identification of the characteristic diffusion length, l , with half-particle size is basically correct.

We also compared the values of D for pure phases 2 and 2L obtained and refined in this work with the component diffusion coefficient of Li ions (D_0) in the HOPG electrode determined by quasi-elastic neutron scattering (QENS) reported by Kim et al. [37]. This technique allowed for direct determination of D_0 at high temperatures. The activation energy was estimated as 0.35 eV. A linear extrapolation of the related plots to room temperatures results in D_0 evaluated as 4.1×10^{-9} and $8.9 \times 10^{-9} \text{ cm}^2 \text{ s}^{-1}$. These values are marked by the broken lines in Fig. 7. Note that for pure phases, the chemical diffusion coefficient, D , is indistinguishable from D_0 [19]. Figure 7 shows that the values of D_0 estimated from QENS of the HOPG electrode deviate from the related values of D of our composite, powdery electrode by less than an order of magnitude. Note, however, that the value of D_0 reported by Kim et al. for lithiated graphite phase 2 correlates with the jump length of the Li ion between two neighboring sites on the basal grapheme plane (0.48 nm), whereas transport of the Li ions, characterized by the chemical diffusion coefficient obtained from the Fickian dynamics, correlates with half of the particle size, 7.5 μm . Thus, two principally different techniques, PITT and QENS, result in similar values of diffusion coefficients despite the fact that the related characteristic diffusion lengths differ by an immense factor of 15,000. This striking effect certainly validates the method of determination of the chemical diffusion coefficient by PITT, in general, and its refinement, based on the concept of mixed diffusion-kinetic limitations during Li-ion intercalation and deintercalation, in particular.

Finally, we conclude that the pseudo-Cottrellian approach, when combined with the lattice gas model, correctly describes the appearance of a minimum in D near the standard potential (i.e., close to the peak of C_{dif}). In contrast, although the estimated value of D from the moving boundary model appeared to be very close to that which followed from the pseudo-Cottrellian approach, the moving boundary model fails to interpret values of D , which are lower by several orders of magnitude than those for the pure phases 2 and 1.

The mismatch between the accessible rate constants of different kinetic stages of phase transition and the characteristic time windows of the electrochemical techniques

The mismatch between the accessible rate constants of different kinetic stages of phase transition and the characteristic time windows of the electrochemical techniques

used is important to the realization of why these techniques reflect differently the kinetics of phase transition during intercalation. In “Non-equilibrium free energy curves during phase transition caused by ion insertion,” we saw that cyclic voltammograms, at relatively high scan rates, are mainly controlled by slow solid-state diffusion and large ohmic drops, which considerably increase the range of potentials in which phase–phase transition takes place. What happens when the scan rate decreases to several microvolts per second and solid-state diffusion ceases to be the relevant RDS? As earlier reported [15], peaks of cyclic voltammograms become progressively narrower, as the scan rate decreases, but the ideal (quasi-equilibrium) behavior of the type shown in Fig. 3b has never been reached, so that one of the possible relaxation processes becomes rate-determining. From the free energy profile shown in Fig. 1, it can be easily seen that an increase in electrode polarization reduces the energetic barrier, so that conventional Butler–Volmer kinetics (here, slow interfacial ion transfer) can control the rate of phase transition. Examples illustrating this possibility have been abundantly presented elsewhere [15, 18, 19].

One can easily imagine an alternative mechanism for the energy barrier reduction. From the analysis of chronoamperometric response during phase transition, we found evidence for the nucleation and growth step to be RDS at the beginning of this transition. The simplest way to take this effect into account to predict the shape of cyclic voltammetric curves is to assume that phase transition may be initiated by a small number of intercalation sites near the electrode/solution boundary, which effectively reduces the energetic barrier (note that the free energy curves in Fig. 1 are those for the unit intercalation site) [10, 15]:

$$C_{\text{dif}}/fQ_m = (\omega/2\pi f\nu)(1-x) \exp(-nE_a/kT). \quad (14)$$

Here, nuclei of the new phase contain n sites only, which reduces the energy barrier, as compared to the case when nucleation occurs on the whole variety of accessible intercalation sites. The characteristic frequency of nucleation process and scan rate are denoted by ω and ν , respectively. The term $(1-x)$ has the meaning of a statistical factor that controls the availability of intercalation sites to be filled as phase transition proceeds. Differential capacity curves were calculated with the use of Eq. 14 and are further numerically integrated to model charging and discharging ($E-E_0$) vs x curves (see broken lines in Fig. 2). It is seen that, indeed, both intercalation and deintercalation begin before reaching the inflection point of the N-shaped curve, which demonstrates the decrease in the energetic barrier due to the small droplet formation of the new phase. Notice, however, that the model proposed (Eq. 14) assumes small droplet formation throughout the *entire phase transition*, whereas the related chronoampero-

metric response (Fig. 5) shows its occurrence only at the beginning of the transition, and within a limited period of time. We are currently trying to understand this disparity by analysis of the potential dependences of D .

Until now, we have compared the ability of CV and small-potential step techniques to reflect RDS of phase transitions during ion insertion. GITT technique can be equally used to obtain C_{dif} and D vs x relationships. The latter quantity can be easily calculated from the plots of potential vs square root of time (I = current pulse applied), using the following simple expression for τ_d :

$$\tau_d = \frac{\pi}{4I^2} \left[C_{\text{dif}} \left(\frac{dE}{dt^{1/2}} \right) \right]^2 \quad (15)$$

The calculated D vs x curves both from Eqs. 15 (GITT) and 13 (PITT) are shown in Fig. 8a and b for Li insertion and deinsertion to/from a composite graphite electrode, respectively. It is clearly seen that GITT ensures a closer approach to the spinodal domain compared to that reached by PITT. This conclusion is in excellent agreement with what followed from the analysis of the numerical results on the basis of the phase field model [3]. The major reason for a higher deviation of the results obtained by PITT from the equilibrium behavior is due to the insufficiently small potential increments used (many phase transitions in intercalation electrodes occur within several tens of millivolts only) and the insufficient time for equilibration after the steps. The difference in accuracy obtained by both techniques for the determination of D can be viewed, alternatively, as a better agreement between the required accessible diffusion rate constant (here, the diffusion time constant), which is related to a small concentration

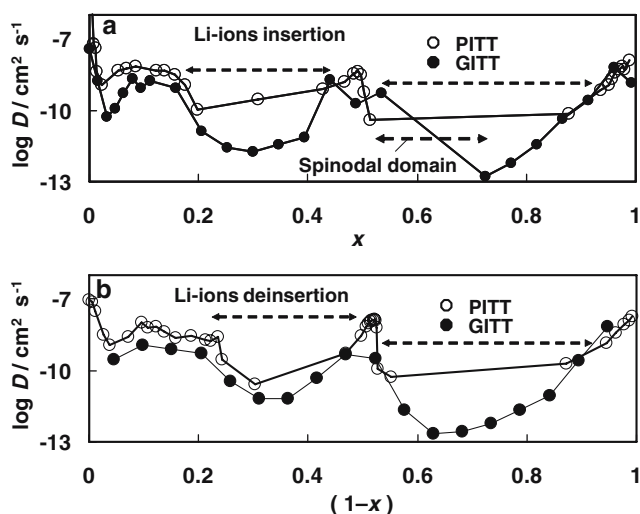


Fig. 8 Comparison between the plots of the chemical diffusion coefficient, $\log D$, as a function of the intercalation level, x [intercalation, (a)], or $(1-x)$ [deintercalation, (b)], obtained for a composite graphite electrode by PITT and GITT, as indicated

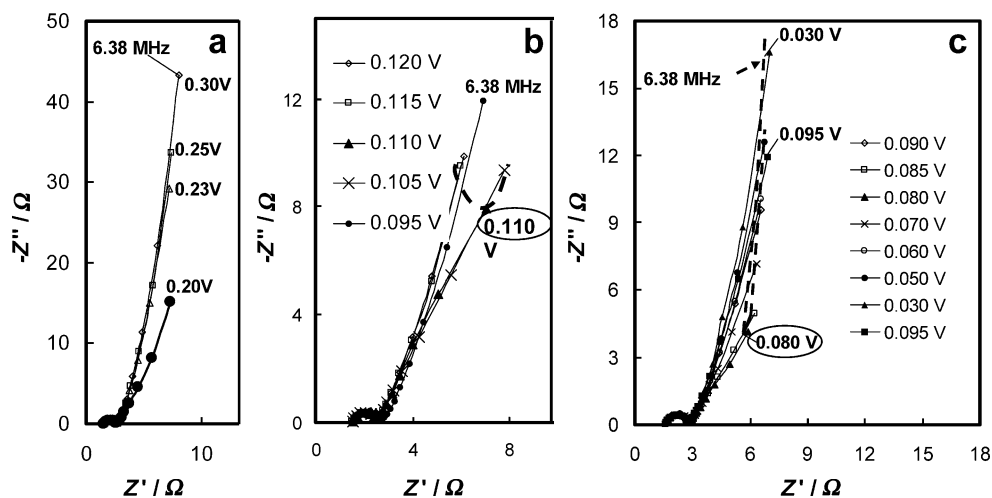
increment and the characteristic window time of the pulsed galvanostatic experiment as compared to the pulsed potentiostatic experiment. Under the condition of a steep concentration gradient, it is simpler to vary the concentration by pulsed current than by pulsed potential.

Another unexpected conclusion drawn from comparison of curves in Fig. 8a and b is that Li-ion deintercalation from lithiated graphite occurs faster than lithiation, so that the width of the related spinodal domain is narrower. Indeed, we did not observe a rising portion of current with time (domain II) during deintercalation of Li ions from LiC_6 (phase 1) to form a more dilute phase LiC_{12} (phase 2). A possible reason for this is that lithiated graphite is subjected, to a certain degree, to self-discharge, i.e., to spontaneous deintercalation. This may well facilitate the formation of a less concentrated phase in the bulk of the more concentrated one, as compared to the opposite process of intercalation.

Finally, in view of the data presented above, we wish to discuss to what extent EIS technique is suitable for characterizing processes that relate to phase transition. Figure 9a, b, and c shows families of impedance spectra during lithiation of a graphite electrode across diluted phase I/phase IV, phase III/phase II, and phase II/phase I transitions, respectively (compare with potential domains of the related CV peaks C, B, and A, respectively, as shown in Fig. 4). As noted in the experimental section, before the measurement of impedance at constant applied potentials, they were preliminarily polarized at the same potentials for a period of 20–30 min. Examining the low-frequency domain of Nyquist plots in Fig. 9b and c, attention should be paid to the fact that the broken line crossing through $-Z''$, Z' points to the lowest measurable frequency of 6.38 MHz and exhibits a deep minimum in $-Z''$ at the potentials 0.110 and 0.080 V (vs Li/Li^+), respectively, i.e., at the potentials at which phase transitions take place. This is hardly accidental, as $-Z'' = (\omega C_{\text{dif}})^{-1}$ is inversely proportional to C_{dif} , the latter showing clear maxima in the related potential ranges of the CV curve (compare with peaks B and A, respectively, in Fig. 4). There is a certain qualitative similarity between the C_{dif} obtained from low-frequency impedance and that obtained from CV, PITT, or GITT. A relatively small change in the Li concentration for the diluted phase I/phase IV transition, and hence not a suitably small potential increment, does not allow for the direct observation of this effect in Fig. 9a.

Impedance technique is usually used for electrochemical systems that can reach true equilibrium state. Then, by perturbing the system from true equilibrium by a small ac current (or potential) at a variety of frequencies, one can identify the various relaxation processes (such as charge transfer, diffusion, etc.) that are the RDS in each characteristic frequency domain. Obviously, the process of first-

Fig. 9 Families of impedance spectra measured from composite graphite electrode at different potentials in the vicinity of the following phase transitions: diluted phase 1→phase 4 (a), phase 3→phase 2 (b), and phase 2→phase 1 (c). Broken lines connect the $-Z''$ measured at the lowest frequency of 3.68 MHz. The minimum values of $-Z''$ fall on potentials marked by the elliptic circles, which are the potentials of the related CV peaks



order phase transition does not imply true thermodynamic equilibrium states, as was emphasized when analyzing the shape of nonequilibrium free energy curves. However, as the time required to measure the entire impedance spectrum was about 15 min, which is much shorter than the time lapse of, e.g., domain IV, this spectrum can be more or less considered as stationary with respect to long-time advancement of the phase transition process. In other words, impedance spectra measured at different potentials across the phase transition reaction correspond to different periods of time of the chronoamperometric response (Fig. 5), and hence, to different instantaneous intercalation levels. For this reason, there should be qualitative correspondence between EIS data and that of, for example, PITT. Under proper magnification of data in Fig. 9b and c, one could note a tendency to form convexity in the low-frequency domain of the spectrum at the potential (or time) at which nucleation domain II appears. High-frequency measurements are even more reliable compared to those in the low-frequency domains, as stationary conditions are fulfilled better. Measurements of impedance at high-frequencies provide truly unique information on ohmic drops, ion transport across surface films, interfacial ion transfer, etc., which can be hardly obtained by PITT or GITT. On the other hand, in view of perturbing the condition of the stationary state at low frequencies, the ability to separate and differentiate between the different relaxation steps deteriorates, compared to that of PITT and GITT. For this reason, combined application of CV, PITT, GITT, and EIS provides the best information on the mechanism of phase transitions, as has been repeatedly emphasized in our previous work.

Conclusion

To summarize, we discuss the phenomenon of first-order phase transition induced by electrochemical intercalation of

Li ions into composite graphite electrodes in the framework of a mean-field approximation to the lattice gas model. Highly attractive interactions between intercalation sites result in the appearance of a large peak (hump) on a nonequilibrium free energy curve, which cannot be overcome in a purely equilibrium-type manner. Phase transition occurs at sufficiently large electrode polarizations under kinetic control. Electroanalytical techniques applied to the study of such phase transitions, even when adequately adapted, are still different in terms of their ability to distinguish between the possible RDS of the phase transition process. This can be viewed as a mismatch between the required accessible rate constants of the kinetic stages of phase transition and the characteristic time windows of the different electrochemical techniques. Note that this disparity is not trivial, and exact analysis can be performed only by a combined application of a number of electroanalytical techniques in a single study. The most inclusive information on the sequence of the RDS during phase transition can be obtained by the application of PITT with a small potential step. On the other hand, when comparing the respective abilities of GITT and PITT to ensure determination of reliable chemical diffusion coefficients, the former technique certainly has a practical advantage over the latter. Application of EIS for the characterization of intercalation processes is most appropriate if the focus is on the high-frequency domains of the spectra, which is related to fast processes. Low-frequency impedance may well correspond to different intercalation levels of the electrode; however, observation of the characteristic peak-shaped potential dependence of $-Z_{\omega \rightarrow 0}$, with the minimum occurring in the vicinity of the related CV peak, is important to ensure that both techniques provide reliable results.

Acknowledgment Partial support for our studies on transport phenomena was obtained from the GIF (German–Israel Foundation).

References

1. Bruce PG (1995) Solid state electrochemistry. Cambridge University Press, pp 1
2. Van Schalkwijk W, Scrosati B (eds) (2002) Advances in lithium-ion batteries. Springer, Berlin Heidelberg New York, p 524
3. Han BC, Van der Ven A, Morgan D, Ceder G (2004) *Electrochim Acta* 49:4691
4. Dahn JR (1991) *Phys Rev B* 44:9170
5. Ohzuku T, Iwakoshi Y, Sawai K (1993) *J Electrochem Soc* 140:2490
6. Winter M, Besenhard JO (1999) In: Besenhard JO (ed) Handbook of battery materials. Wiley-VCH, Weinheim, p 383
7. Levi MD, Levi EA, Aurbach D (1997) *J Electroanal Chem* 421:89
8. McKinnon WR, Haering RR (1987) Modern aspects in electrochemistry, vol 15. Plenum, New York, p. 235
9. Feldberg SW, Rubinstein I (1988) *J Electroanal Chem* 240:1
10. Vorotyntsev MA, Badiali JP (1994) *Electrochim Acta* 39:289
11. Funabiki A, Inaba M, Abe T, Ogumi Z (1999) *J Electrochem Soc* 146:2443
12. Shin Heon-Cheol, Pyun Su-II (1999) *Electrochim Acta* 44:2235
13. Shin Heon-Cheol, Pyun Su-II (1999) *Electrochim Acta* 45:489
14. Levi MD, Aurbach D (1997) *J Phys Chem B* 101:4641
15. Levi MD, Aurbach D (1999) *Electrochim Acta* 45:167
16. Levi MD, Salitra G, Markovsky B, Teller H, Aurbach D (1999) *J Electrochem Soc* 146:1279
17. Levi MD, Gamolsky K, Heider U, Oesten R, Aurbach D (1999) *J Electroanal Chem* 477:32
18. Markevich E, Levi MD, Aurbach D (2005) *J Electroanal Chem* 580:231
19. Levi MD, Markevich E, Aurbach D (2005) *Electrochim Acta* 51:98
20. Levi MD, Markevich E, Aurbach D (2005) *J Phys Chem B* 109:7420
21. Levi MD, Markevich E, Wang C, Koltypin M, Aurbach D (2004) *J Electrochem Soc* 151:A848
22. Simons W, Gonnissen D, Hubin A (1997) *J Electroanal Chem* 433:141
23. Gonnissen D, Simons W, Hubin A (1997) *J Electroanal Chem* 435:149
24. Fleischmann M, Thirsk HR (1963) In: Delahay P, Tobias CW (eds) Advances in electrochemistry and electrochemical engineering, vol 3. Wiley, New York
25. Bewick A, Fleischmann M, Thirsk HR (1962) *Trans Faraday Soc* 58:2200
26. Levi MD, Markevich E, Wang C, Aurbach D (2007) *J Electroanal Chem* 600:13
27. Montella C (2002) *J Electroanal Chem* 518:61
28. Bard AJ, Faulkner LR (2001) Electrochemical methods: fundamentals and applications, 2nd edn. Wiley, New York
29. Weppner W, Huggins RA (1978) *Annu Rev Mater Sci* 8:269
30. Wen CJ, Boukamp BA, Huggins RA, Weppner W (1979) *J Electrochem Soc* 126:2258
31. Montella C (2006) *Electrochim Acta* 51:3102
32. Deiss E (2002) *Electrochim Acta* 47:4027
33. Eftekhari A (2005) *Electrochim Acta* 50:2541
34. Vorotyntsev MA, Levi MD, Aurbach D (2004) *J Electroanal Chem* 572:299
35. Levi MD, Demadrille R, Pron A, Vorotyntsev MA, Gofer Y, Aurbach D (2005) *J Electrochem Soc* 152:E61
36. Funabiki A, Inaba M, Ogumi Z, Yuasa S, Otsuji J, Tasaka A (1998) *J Electrochem Soc* 145:172
37. Kim HJ, Magerl A, Fischer JE, Vaknin D, Heitjans P, Schirmer A (1993) In: Bernier P et al (eds) Chemical physics of intercalation II. Plenum, New York, p 355